Supplemental Information

The Genomic Landscape of Endocrine-Resistant Advanced Breast Cancers

Pedram Razavi, Matthew T. Chang, Guotai Xu, Chaitanya Bandlamudi, Dara S. Ross, Neil Vasan, Yanyan Cai, Craig M. Bielski, Mark T.A. Donoghue, Philip Jonsson, Alexander Penson, Ronglai Shen, Fresia Pareja, Ritika Kundra, Sumit Middha, Michael L. Cheng, Ahmet Zehir, Cyriac Kandoth, Ruchi Patel, Kety Huberman, Lillian M. Smyth, Komal Jhaveri, Shanu Modi, Tiffany A. Traina, Chau Dang, Wen Zhang, Britta Weigelt, Bob T. Li, Marc Ladanyi, David M. Hyman, Nikolaus Schultz, Mark E. Robson, Clifford Hudis, Edi Brogi, Agnes Viale, Larry Norton, Maura N. Dickler, Michael F. Berger, Christine A. Iacobuzio-Donahue, Sarat Chandarlapaty, Maurizio Scaltriti, Jorge S. Reis-Filho, David B. Solit, Barry S. Taylor, and José Baselga

Table S1, related to Figure 1: Demographic and clinical characteristics of the study cohort.

	HR^+HER2^- n=1364	HR^+HER2^+ n=166	HR^-HER2^+ n=58	TNBC n=168	p value
Age at Diagnosis					0.001
<40	220 (16.1)	42 (25.3)	11 (19)	36 (21.4)	
40-49	382 (28)	55 (33.1)	17 (29.3)	40 (23.8)	
50-59	392 (28.7)	49 (29.5)	20 (34.5)	50 (29.8)	
≥60	370 (27.1)	20 (12)	10 (17.2)	42 (25)	
Stage at Diagnosis					<0.001
Stage I	429 (31.5)	31 (18.7)	14 (24.1)	47 (28)	
Stage II	401 (29.4)	44 (26.5)	9 (15.5)	54 (32.1)	
Stage III	271 (19.9)	36 (21.7)	14 (24.1)	35 (20.8)	
Stage IV	252 (18.5)	53 (31.9)	21 (36.2)	32 (19)	
Not available	11 (0.8)	2 (1.2)	0 (0)	0 (0)	
Histology					<0.001
Invasive Ductal	1007 (73.8)	136 (81.9)	51 (87.9)	147 (87.5)	
Invasive Lobular	253 (18.5)	15 (9)	3 (5.2)	3 (1.8)	
Mixed Ductal/Lobular	73 (5.4)	8 (4.8)	1 (1.7)	1 (0.6)	
Carcinoma, NOS	18 (1.3)	6 (3.6)	2 (3.4)	3 (1.8)	
Other	13 (0.9)	1 (0.6)	1 (1.7)	14 (8.4)	
Histologic Grade (Primary Tumor)					<0.001
I-Well Differentiated	87 (6.4)	2 (1.2)	1 (1.7)	0 (0)	
II-Moderately Differentiated	382 (28)	26 (15.7)	6 (10.3)	9 (5.4)	
III-Poorly Differentiated	747 (54.8)	120 (72.3)	47 (81)	156 (92.9)	
Not available	148 (10.9)	18 (10.8)	4 (6.9)	3 (1.8)	
Menopausal Status at Diagnosis					0.09
Pre	608 (44.6)	96 (57.8)	29 (50.0)	71 (42.3)	
Peri	82 (6)	7 (4.2)	4 (6.9)	7 (4.2)	
Post	660 (48.4)	61 (36.7)	25 (43.1)	88 (52.4)	
Not Applicable (Male)	8 (0.6)	2 (1.2)	0 (0)	0 (0)	
Not Available	6 (0.4)	0 (0)	0 (0)	2 (1.2)	
Distant Metastasis at last follow-up					
Yes	948 (69.5)	143 (86.1)	49 (84.5)	121 (72)	<0.001

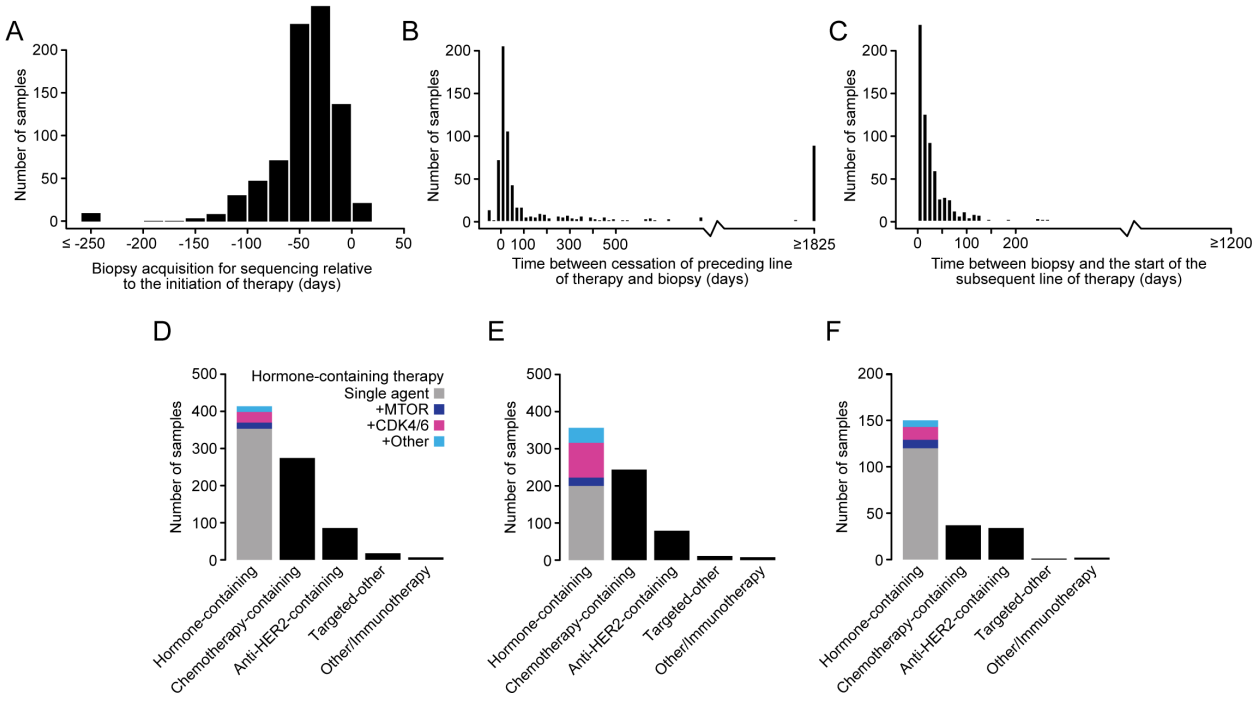

Figure S1, related to Figure 1: Treatment lines and biopsies for prospective sequencing. **(A)** In 912 treatment-naïve tumor specimens acquired prior to the start of therapy, the time in days between biopsy acquisition for sequencing the initiation of therapy is shown. **(B)** For 782 samples sequenced from a biopsy obtained after at least one line of therapy, the time is shown between the cessation of the immediately preceding line of therapy and the biopsy for sequencing. **(C)** For the same post-treatment specimens shown in panel (B), the time between the biopsy for sequencing and the start of the next line of therapy (in days) is shown. **(D)** The distribution of therapy type is shown for the line of therapy directly preceding biopsy for post-treatment specimens. **(E)** As in panel (D) but for the line of therapy directly following the biopsy for sequencing. **(F)** For 224 samples that were acquired on-treatment (184 of which also received prior therapies), the line of therapy during which the biopsy occurred is indicated by category.

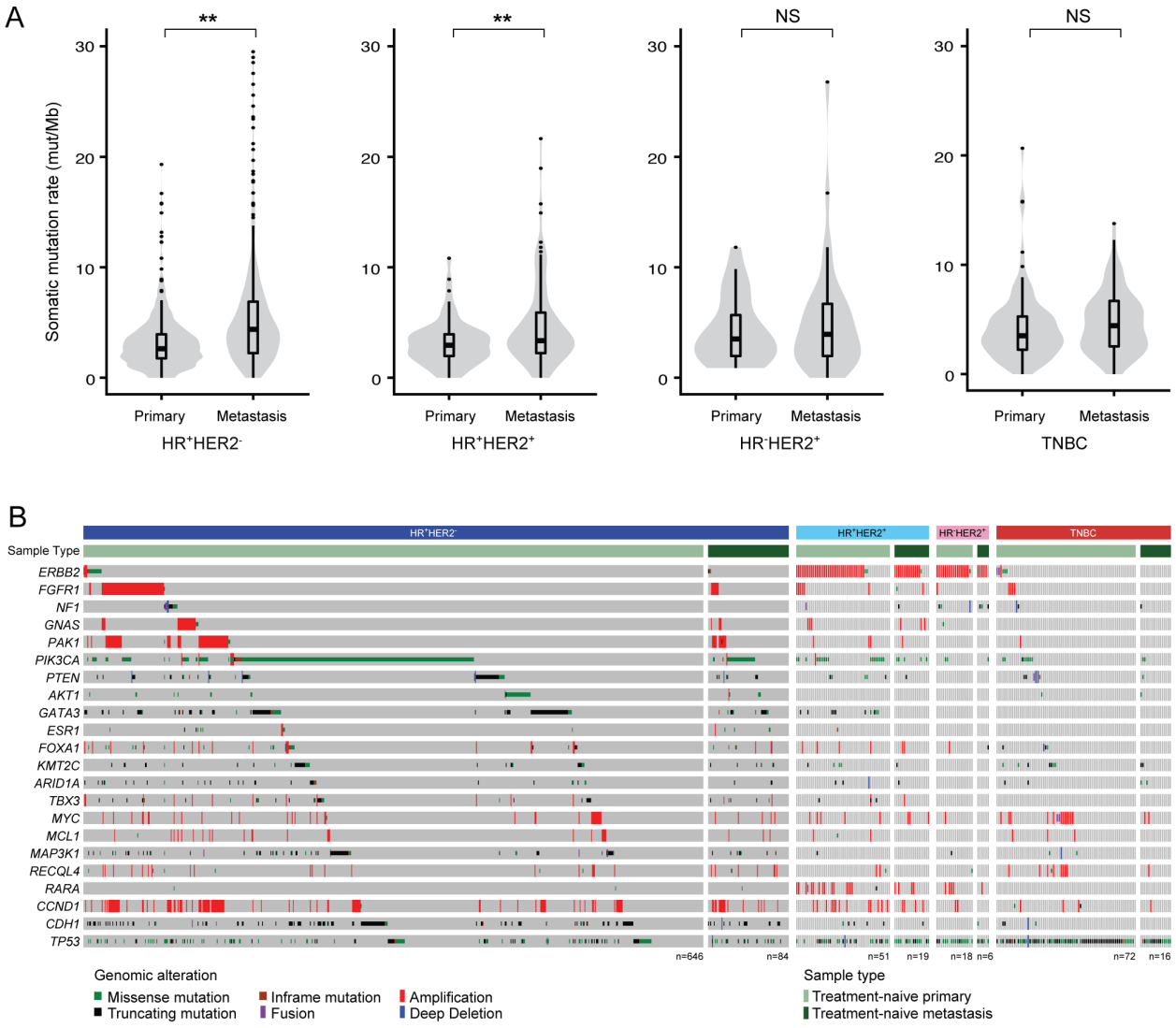
A
Somatic mutation rate (mut/Mb)
**
**
NS
NS
Primary
Metastasis
HR+HER2-
HR+HER2+
HR-HER2+
TNBC
B
Sample Type
ERBB2
FGFR1
NF1
GNAS
PAK1
PIK3CA
PTEN
AKT1
GATA3
ESR1
FOXA1
KMT2C
ARID1A
TBX3
MYC
MCL1
MAP3K1
RECQL4
RARA
CCND1
CDH1
TP53
n=646
n=84
n=51
n=19
n=18
n=6
n=72
n=16
Genomic alteration
Missense mutation
Truncating mutation
Inframe mutation
Fusion
Amplification
Deep Deletion
Sample type
Treatment-naive primary
Treatment-naive metastasis
C
Frequency of affected tumors (%)
HR+HER2- Primary
HR+HER2- Metastasis
HR+HER2+ Primary
HR+HER2+ Metastasis
HR-HER2+ Primary
HR-HER2+ Metastasis
TNBC Primary
TNBC Metastasis

Figure S2, related to Figure 2: (A) Mutational burden in primary and metastatic tumors by receptor subtype. The somatic mutational burden is shown in primary and metastatic specimens by receptor subtype as estimated from prospective sequencing (and shown as mutations per megabase of sequence). Asterisks indicate a statistically significant those modest difference among HR^+HER2^- and HR^+HER2^+ patients. The violin plots represent the distribution of the data. The bottom and top of the boxplot represent the lower and upper quartiles, respectively, and the band near the middle of the box represents the median. The upper whisker represents the upper quartile +1.5 x interquartile range (IQR) and the lower whisker represents the lower quartile - 1.5 x IQR. The dots represent the outliers. **(B and C) Analysis of treatment-naïve primary and metastatic cohorts. (B)** The pattern, frequency, and type of genomic alterations in key breast cancer genes (as shown in Fig. 2A) in 787 treatment-naïve primary tumors (left) compared to 125 treatment-naïve metastatic tumors (predominantly [n=103] *de novo* metastatic disease, right) for each of the four indicated receptor subtypes. **(C)** Comparison of the frequency of alterations in the genes and subtypes in panel (B). No statistically significant changes were evident after correcting for multiple comparisons given the small sample sizes of most comparisons.

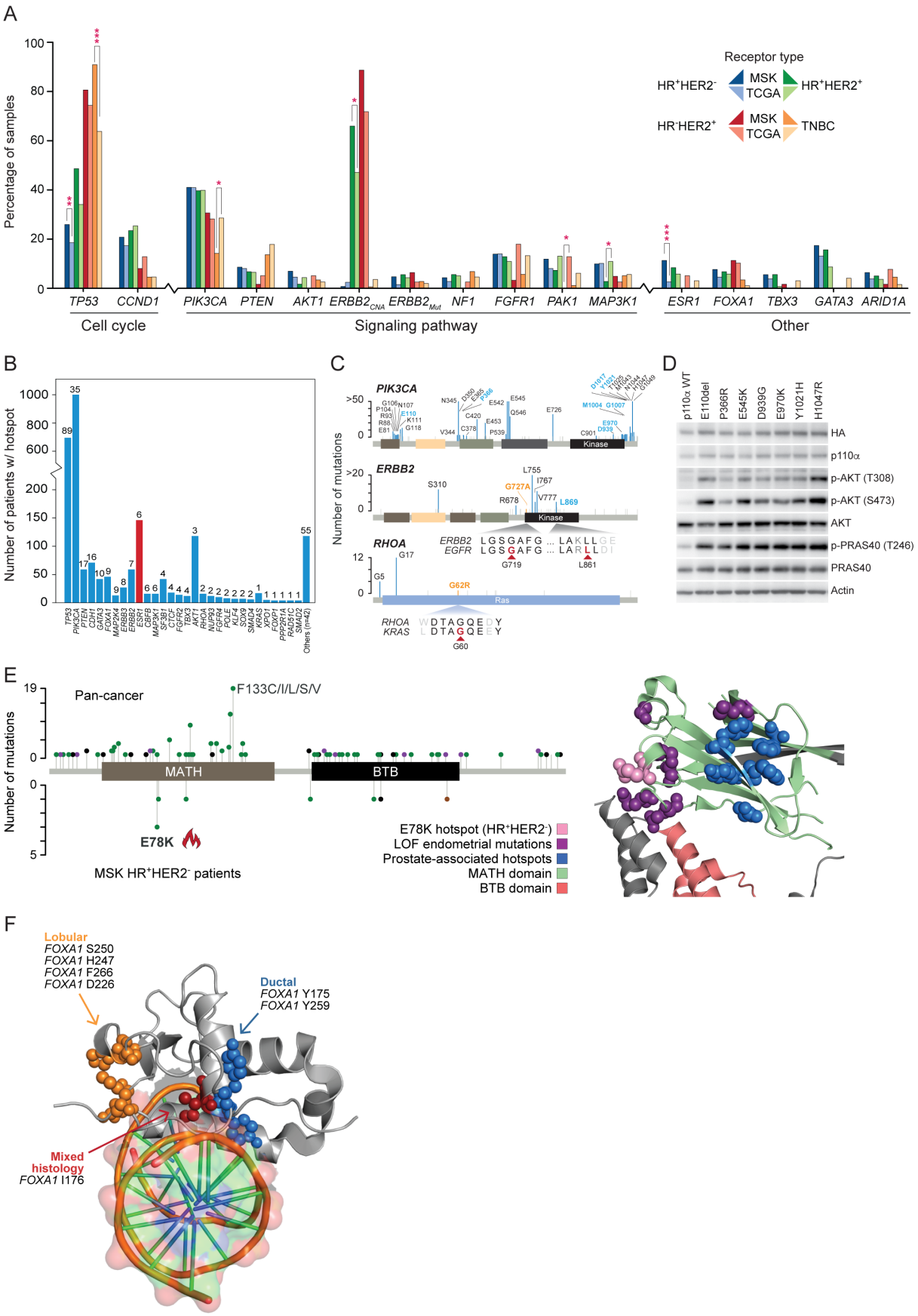
A
Percentage of samples
Receptor type
HR+HER2-
MSK
TCGA
HR+HER2+
HR-HER2+
TNBC
TP53
CCND1
PIK3CA
PTEN
AKT1
ERBB2CNA
ERBB2Mut
NF1
FGFR1
PAK1
MAP3K1
ESR1
FOXA1
TBX3
GATA3
ARID1A
Cell cycle
Signaling pathway
Other
B
Number of patients w/ hotspot
C
PIK3CA
ERBB2
RHOA
Number of mutations
Kinase
Ras
G727A
L869
G62R
G60
D
p110α WT
E110del
P366R
E545K
D939G
E970K
Y1021H
H1047R
HA
p110α
p-AKT (T308)
p-AKT (S473)
AKT
p-PRAS40 (T246)
PRAS40
Actin
E
Pan-cancer
F133C/I/L/S/V
MATH
BTB
E78K
MSK HR+HER2- patients
E78K hotspot (HR+HER2-)
LOF endometrial mutations
Prostate-associated hotspots
MATH domain
BTB domain
F
Lobular
FOXA1 S250
FOXA1 H247
FOXA1 F266
FOXA1 D226
Ductal
FOXA1 Y175
FOXA1 Y259
Mixed histology
FOXA1 I176

Figure S3, related to Figure 2: (A) Gene-level comparisons of alteration rates by receptor subtype. The frequency of alterations in breast cancer genes by receptor subtype in this cohort and the primary untreated breast cancers of The Cancer Genome Atlas study.(Cancer Genome Atlas, 2012) Significant differences are indicated by red asterisks. **(B, C, and D) Driver mutations reveal candidate actionability. (B)** The number of hotspots identified in one of 30 genes are shown as is the number affected patients. *ESR1* is highlighted in red. **(C)** The pattern and frequency of hotspot mutations in *PIK3CA*, *ERBB2*, and *RHOA* are shown. Mutations in blue have not been previously described or studied. Mutations arising at positions paralogous to mutant alleles in closely related family members are indicated below the linear schematic of the relevant gene. **(D)** All five novel *PIK3CA* hotspot mutations identified here induced levels of phosphorylated AKT (T308/S473) and PRAS40 higher than did expression of the wild-type p110a in MCF10A mammary epithelial cells. **(E) *SPOP* E78K mutations in $HR^{+}HER2^{-}$ breast cancers.** A linear schematic of SPOP and its domain structure is shown with the pattern and frequency of somatic mutations from a large pan-cancer cohort (Zehir et al., 2017) and this study cohort of breast cancers (bottom). The E78K hotspot is identified. At right is the three-dimensional structure of SPOP with mutations as indicated in the legend. **(F) Structure of histology-specific hotspots in *FOXA1*.** Hotspots arising in *FOXA1* are either specific to lobular or ductal cancers (orange and blue, respectively) and target different wings of the transcription factor (as bound to DNA) while a single I176 hotspot arises in mixed histology tumors.

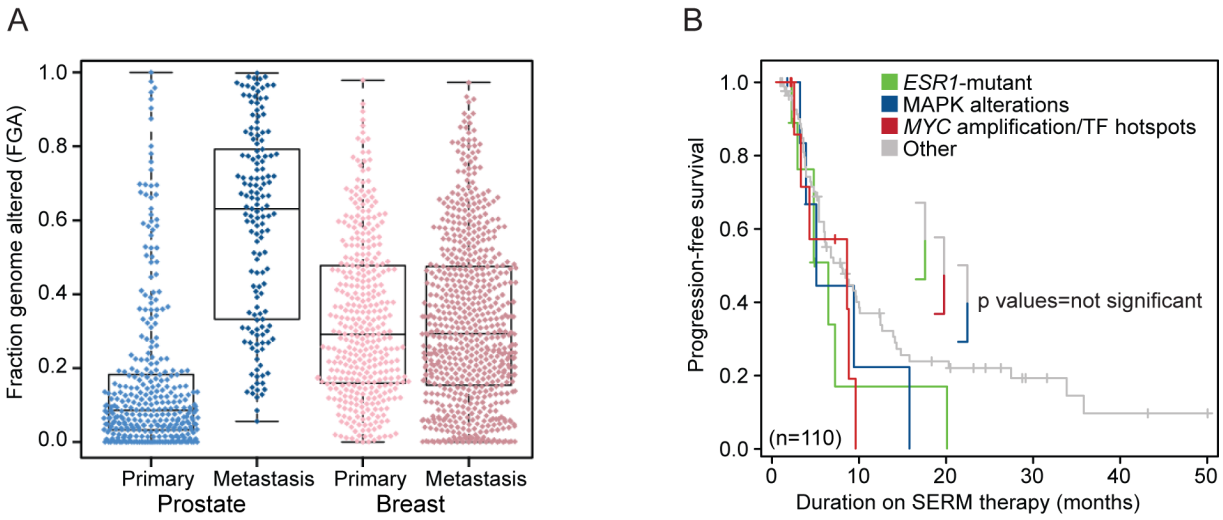

Figure S4, related to Figure 3: (A) Copy number burden by disease state. The overall burden of DNA copy number alterations gnome wide is shown for primary and metastatic prostate and breast cancers. The bottom and top of the boxplot represent the lower and upper quartiles, respectively, and the band near the middle of the box represents the median. The upper whisker represents the upper quartile +1.5 x interquartile range (IQR) and the lower whisker represents the lower quartile - 1.5 x IQR. **(B) Outcomes on first-line SERM therapy and classes of genomic alterations.** Kaplan-Meier curve displaying the progression-free survival of patients receiving first-line SERM alone after their biopsy for prospective sequencing. Genotypic classes are shown as in Figure 3C-D) and outcome is compared to patients whose tumors were wild-type for such lesions (gray). All p value are not significant, log rank test.

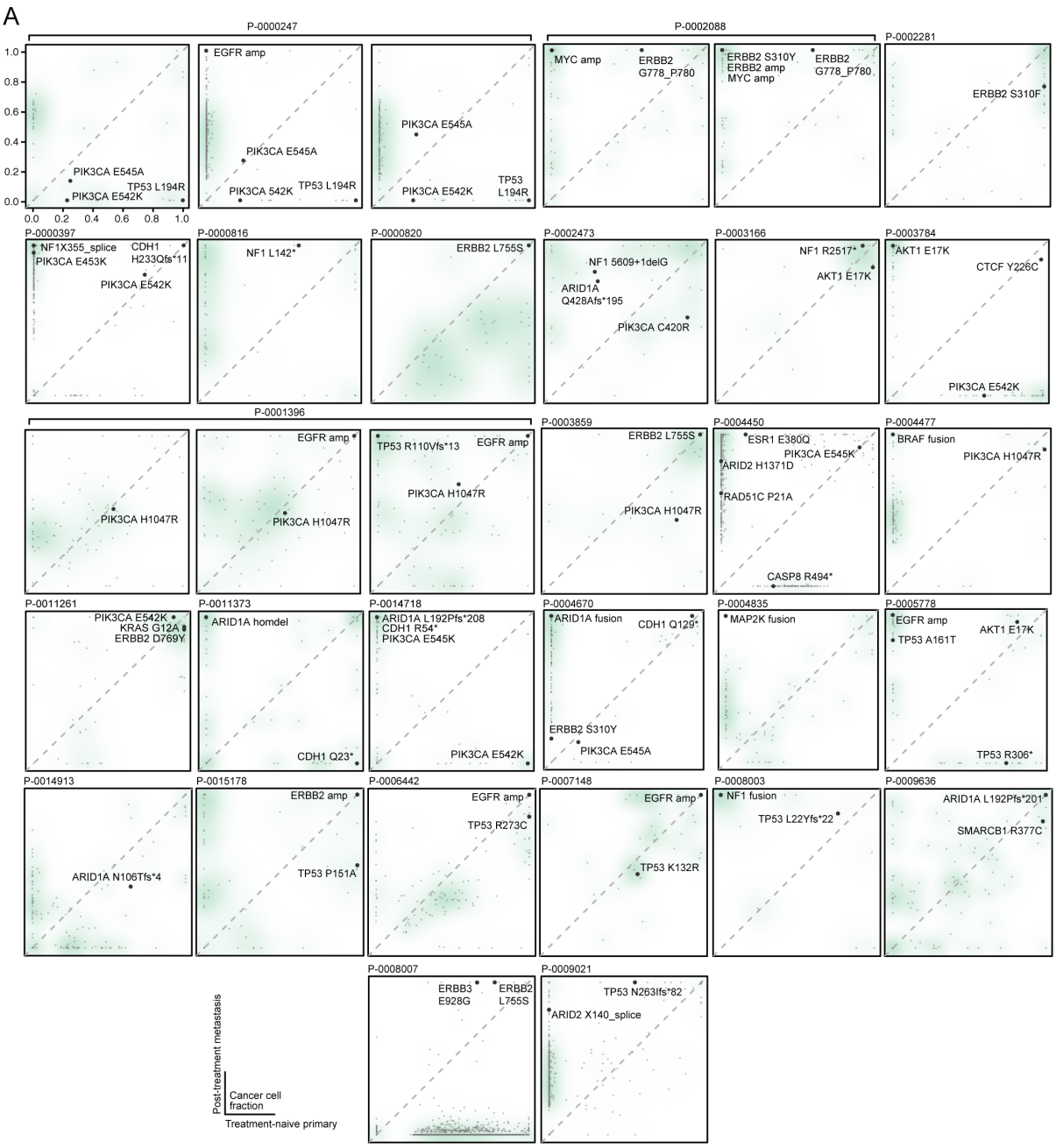
A
P-0000247
P-0002088
P-0002281
P-0000397
P-0000816
P-0000820
P-0002473
P-0003166
P-0003784
P-0001396
P-0003859
P-0004450
P-0004477
P-0011261
P-0011373
P-0014718
P-0004670
P-0004835
P-0005778
P-0014913
P-0015178
P-0006442
P-0007148
P-0008003
P-0009636
P-0008007
P-0009021
Post-treatment metastasis
Cancer cell fraction
Treatment-naive primary
B
TP53 N239D
CDH1 W156Tfs
ERBB3 E928G
TP53 D208N
PIK3CA E545Q
ERBB2 S310Y
ERBB2 L755S
ESR1 Y537S
PIK3CA E545K
Lymph Node (LN)
Cutaneous Metastasis (CM3)
Cutaneous Metastasis (CM4)
Cutaneous Metastasis (CM2)
Cutaneous Metastasis (CM1)
Chest Wall (CW)
Liver Metastasis (LM)
Pleural Disease (PD2)
Pleural Disease (PD1)
Retroperitoneal Metastasis (RM)
Pre-mortem recurrence

Figure S5, related to Figure 4: (A) Additional 27 patients with matched pre- and post-treatment WES. For all patients with matched pairs of treatment-naïve primary and post-treatment metastatic specimens that underwent whole-exome sequencing, the distribution of cancer cell fraction (estimated fraction of cancer cells affected by somatic mutations) are shown. Each box represents a patient (patient identifier as indicated). The x- and y-axes show the treatment-naïve primary and post-treatment metastatic specimens respectively. Green shading represents clusters of somatic mutations at different cancer cell fractions (~1 is clonal). The individual gray points represent all mutations detected. Identified in each patient are both the candidate mechanisms of endocrine therapy resistance and other breast cancer driver mutations in the patients. **(B) Common and private somatic mutational patterns in the autopsy.** Somatic mutations (blue) identified in the whole-exome sequencing of a pre-mortem recurrent cutaneous metastasis and 10 metastatic specimens obtained post-mortem. Shared mutations (common to all sites of disease or common to only subsets of disease sites are shown as are private mutations arising specifically in a single metastatic site but not the others. Driver mutations and those mutations presumed to mediate endocrine resistance (*ERBB2* and *ESR1*) are identified in orange.

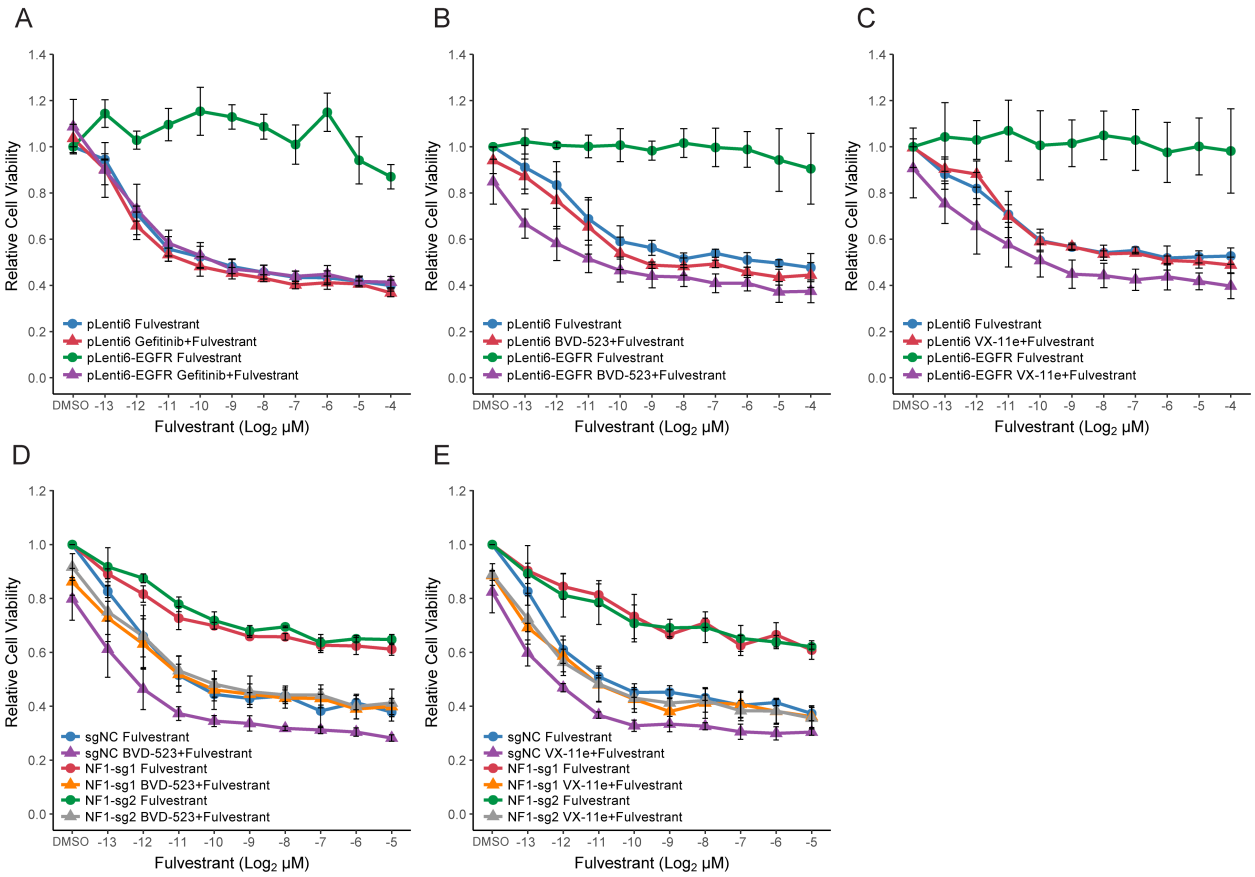

Figure S6, related to Figure 5: Functional validation of MAPK activation as mechanism of resistance to endocrine therapy: (A-C) Cell viability of MCF7 stably transfected with pLenti6 mock control or pLenti6-EGFR upon treatment with fulvestrant or fulvestrant + gefitinib (A), fulvestrant + BVD-523 (B), or fulvestrant + VX-11e (C). **(D and E)** Cell viability of two independent NF1 knock out clones treated with fulvestrant or fulvestrant + BVD-523 (D), or fulvestrant + VX-11e (E). Error bars represent standard deviations.